Surface calculations with asymptotically long-ranged potentials in the full-potential linearized augmented plane-wave method

Lin-Hui Ye

Department of Electronics, Key Laboratory for the Physics and Chemistry of Nanodevices, Peking University, Beijing 100871, Peoples Republic of China

(Received 11 July 2015; revised manuscript received 11 August 2015; published 15 September 2015)

Although the supercell method has been widely used for surface calculations, it only works well with short-ranged potentials, but meets difficulty when the potential decays very slowly into the vacuum. Unfortunately, the exact exchange-correlation potential of the density functional theory is asymptotically long ranged, and therefore is not easily handled by use of supercells. This paper illustrates that the authentic slab geometry, another technique for surface calculations, is not affected by this issue: It works equally well with both short- and long-ranged potentials, with the computational cost and the convergence speed being essentially the same. Using the asymptotically long-ranged Becke-Roussel'89 exchange potential as an example, we have calculated six surfaces of various types. We found that accurate potential values can be obtained even in extremely low density regions of more than 100 Å away from the surface. This high performance allows us to explore the asymptotic region, and prove with clean numerical evidence that the Becke-Roussel'89 potential satisfies the correct asymptotic behavior for slab surfaces, as it does for finite systems. Our finding further implies that the Slater component of the exact exchange optimized effective potential is responsible for the asymptotic behavior, not only for jellium slabs, but for slabs of any type. The Becke-Roussel'89 potential may therefore be used to build asymptotically correct model exchange potentials applicable to both finite systems and slab surfaces.

DOI: 10.1103/PhysRevB.92.115132 PACS number(s): 71.15.−m, 31.15.E−, 73.22.Pr

I. INTRODUCTION

Most solid surface calculations by density functional theory (DFT) make use of the supercell approach, within which the surface is simulated by periodic slabs of finite thickness separated by vacuum spaces. To avoid artificial interslab interactions, the size of the vacuum shall be large enough to ensure that the Kohn-Sham orbitals, the electron density, and the Kohn-Sham effective potential all decay to sufficiently low values in the middle of the vacuum. How difficult this requirement can be to fulfill depends on the exchange-correlation potential but not on the orbitals or the density, since in any case the latter two quantities always decay exponentially. So far, dominant surface calculations make use of the local density approximation (LDA) or generalized gradient approximations (GGA). Since these potentials also decay exponentially, the vacuum thickness can be chosen as small as about 20 Å.

Unfortunately, the exponential decay of the LDA/GGA potentials is physically incorrect. For either semi-infinite materials or slabs of finite thickness, v_{xc} is expected to be long ranged. For an example, Lang and Kohn suggests that the exact v_{xc} of semi-infinite metals asymptotically approaches the classical image potential far away from the surface [1]:

$$v_{xc}(z) \xrightarrow{z\to\infty} -\frac{1}{4z}. \tag{1}$$

For semi-infinite semiconductors and insulators Almbladh and von Barth suggest similar $-1/z$ decay [2]. However, these long-ranged behaviors of the exact v_{xc} have been widely ignored in existing surface calculations because the majority of works use the erroneously short-ranged LDA/GGA. Missing the long-range tail of v_{xc} leads to too high orbital energies, with the error being the most well known for surface states. In particular, for image states explicit correction for the missing tail of v_{xc} must be taken into consideration [3].

The importance of ensuring the correct asymptotic behaviors of v_{xc} is best illustrated by the deviation of the "IP theorem," which claims that the orbital energy of the highest occupied state must be equal to the exact ionization potential (IP) [2,4]. Practical calculations reveal that the IP's evaluated by the LDA/GGA eigenvalues are typically 0.1 eV to a few eV too small, which partly depend on the size of the band gap. For atoms and molecules, van Leeuwen and Baerends [5] have shown that by pasting the missing tail of v_{xc} to the GGA the IP errors are drastically reduced. Since then, many asymptotically long-ranged v_{xc}'s have been extensively studied for finite systems [5–23].

For solid surfaces, asymptotically long-ranged potentials are rarely used since such potentials are not easily handled by a supercell. This is because, (i) due to the slow decay of the potential, the supercell has to include much larger vacuum space; and (ii) for clean representation of the asymptotically behavior, the requirement on the completeness of the basis set is usually much more stringent. Both reasons lead to a drastic increase in the size of the basis set. As an illustrative example, the exact exchange [24,25] optimized effective potential [26,27] (EXX-OEP, also denoted as exact exchange in the following) of graphene has been calculated [28] by the supercell approach, in which 16 000 plane waves are used only to marginally reveal the asymptotic behavior of the v_x. Therefore, for other realistic surfaces the computational cost may easily become unmanageable.

The above supercell problem affects a wide range of applications, including asymptotically correct potentials [5–15], long-range corrected hybrid functionals [16–23], and GW approximation [29], and may become especially serious for the latter two due to the nonlocal feature of the potential

and the self-energy. Moreover, the problem is not unique to the plane-wave method, but also exists in the full-potential linearized augmented plane-wave (FLAPW) method which also uses plane waves as vacuum basis functions. In fact, the problem is even more agonizing in FLAPW because the number of plane waves is limited (since otherwise basis set superposition error would arise), which makes the requirement of basis set completeness even harder to achieve.

To facilitate the use of asymptotically correct potentials [5–23] for surface calculations, the efficiency of the vacuum basis set needs to be substantially improved. In the FLAPW method, it has been shown [30,31] that the linearization technique traditionally used for the muffin tins can also be extended to the vacuum region. This allows for the plane waves to be replaced by exponentially decaying functions to form a new, superefficient vacuum basis set. Following the removal of the plane waves, the artificial supercell periodicity perpendicular to the surfaces becomes obsolete, and is thus abandoned so that all vacuum functions now decay naturally. Now that there is only one "suspended slab" in space, the interslab interactions are completely avoided.

This so-called "authentic slab geometry" [30,31] is a more intuitive way for surface calculations. It is highly efficient, with its accuracy being protected by the linearization technique. So far, the authentic slab geometry has only been used with LDA/GGA, while no attempt has been made for using asymptotically long-ranged potentials. The purpose of this work is to illustrate that, within the authentic slab geometry, calculations with asymptotically long-ranged potentials meet no technical difficulty. The size of the FLAPW basis set remains the same, and the computational cost and the convergence speed are also similar no matter whether short- or long-ranged potentials are used.

For illustration, we use the asymptotically long-ranged Becke-Roussel'89 (BR89) exchange potential [32] to calculate six surfaces of various types. We found that accurate potential values can be obtained even in extremely low density regions of more than 100 Å away from the surfaces. The asymptotic behavior of BR89 is known [32] to be correct for finite systems but has not been discussed previously for solid surfaces. The high performance of the authentic slab geometry allows us to investigate the asymptotic region, which provides clean numerical evidence that for slab surfaces the asymptotic behavior of BR89 is also correct. Our finding further implies that the Slater component of the EXX-OEP is responsible for the asymptotic behavior, not only for jellium slabs [33], but in fact for slabs of arbitrary types.

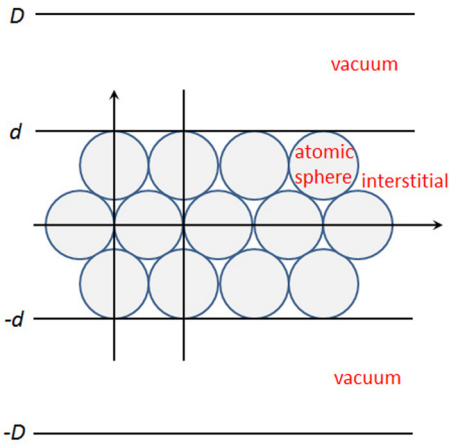

FIG. 1. (Color online) Schematic illustration of the authentic slab geometry of the FLAPW method.

Judged by the above results, the authentic slab geometry provides an excellent, unified method for surface calculations with both short-ranged and asymptotically long-ranged potentials.

The rest of this paper is organized as follows: First we review the fundamentals of the authentic slab geometry and the BR89 exchange potential. Details of the implementation of this potential to the NU-FLAPW code [34] can be found elsewhere [35]. The numerical results are presented afterwards together with discussions which also offer implications to the supercell approach. At the end of this paper we summarize our work. Unless explicitly specified, all quantities use atomic units.

II. TECHNICAL DETAILS

A. The authentic slab geometry

The authentic slab geometry is schematically shown in Fig. 1. The partition of the space into the muffin tins and the interstitial region is the same as in the standard FLAPW method, except that the vacuum spaces are separated from the interstitial and are treated differently. The boundaries of the interstitial locate at $\pm d$, and the thickness of the top and bottom vacuums is $D - d$, which can be tuned by varying D. For more details about the authentic slab geometry refer to Refs. [30,31].

The basis functions take the following hybrid form:

$$\varphi_{\mathbf{g}}(\mathbf{r}) = \begin{cases} \frac{1}{\sqrt{\Omega}} e^{i\mathbf{g}\cdot\mathbf{r}} & \text{(interstitial)} \\ \sum_{lm}[a_l(\mathbf{g})u_l(r_\alpha) + b_l(\mathbf{g})\dot{u}_l(r_\alpha)]Y_{lm}(\hat{\mathbf{r}}_\alpha)Y^\star_{lm}(\hat{\mathbf{g}}) & \text{(muffin tins)} \\ [A_v(\mathbf{g}_\parallel)u_{\mathbf{g}_\parallel}(z) + B_v(\mathbf{g}_\parallel)(z)\dot{u}_{\mathbf{g}_\parallel}(z)]e^{i\mathbf{g}_\parallel\cdot\mathbf{r}_\parallel} & \text{(vacuum).} \end{cases}$$

The a_l, b_l, A_v, B_v coefficients ensure the basis functions to be smoothly continuous at all muffin-tin and interstitial boundaries. In the above equations, $\mathbf{g} = \mathbf{k} + \mathbf{G}$, and $\mathbf{g}_\parallel$ and $\mathbf{r}_\parallel$ are the in-plane components of $\mathbf{g}$ and $\mathbf{r}$, respectively.

Within the muffin tins and the interstitial the basis functions are the same as in standard FLAPW. In the vacuums, the exponentially decaying function $u_{\mathbf{g}_\parallel}$ is generated by

$$\left(\frac{g_\parallel^2}{2} - \frac{1}{2}\frac{d^2}{dz^2} + v_0(z) - E_v\right)u_{\mathbf{g}_\parallel}(z) = 0 \tag{2}$$

with E_v being the prechosen vacuum energy parameter, and $v_0(z)$ the z-dependent, xy-averaged total Kohn-Sham potential. The other exponentially decaying function $\dot{u}_{\mathbf{g}_\parallel}$ serves as the linearization correction to $u_{\mathbf{g}_\parallel}$ and is generated by another equation corresponding to the first energy derivative of Eq. (2). The combined use of both $u_{\mathbf{g}_\parallel}$ and $\dot{u}_{\mathbf{g}_\parallel}$ in the vacua is in analog to that of u_l and $\dot{u}_l$ in the muffin tins.

All Kohn-Sham orbitals are expanded by

$$\psi_{n\mathbf{k}}(\mathbf{r}) = \sum_{\mathbf{G}}^{G\leqslant G_{\max}} z_{n\mathbf{k}}(\mathbf{G})\varphi_{\mathbf{g}}(\mathbf{r}). \tag{3}$$

The plane-wave cutoff $G_{\max}$ determines the size of the FLAPW basis set. The choice of its value is usually guided by

$$G_{\max} R_{\mathrm{MT}} \sim 8. \tag{4}$$

In principle, the vacuum thickness $D-d$ can be set to any value. With LDA/GGA, $D-d \sim 10$ Å is often large enough to ensure the orbitals, the electron density, and the potentials drop to zero at the vacuum edges. On the other hand, for slowly decaying potentials like $v(z) \sim -1/z$ the vacuum thickness has to be chosen much larger, as will become clear in our following results. Note that the increase of the vacuum thickness does not affect the value of $G_{\max}$. This is because the plane waves are used only to represent the interstitial region, and therefore the size of the basis set is determined by the fixed interstitial thickness of $2d$, but not affected by the thickness of the vacua which use the exponentially decaying basis functions. Therefore, calculations with short- and long-ranged potentials take essentially the same amount of time, and the convergence speed is also similar.

B. The Becke-Roussel'89 exchange potential

The Becke-Roussel'89 potential [32] only contains the exchange part. The most notable feature of v_x^{BR} is that it simulates the exchange hole of the hydrogenic atom rather than that of the uniform electron gas. For the σ spin:

$$v_{x,\sigma}^{\mathrm{BR}}(\mathbf{r}) = -\frac{1}{b_\sigma(\mathbf{r})}\left(1 - e^{-x_\sigma(\mathbf{r})} - \frac{1}{2}x_\sigma(\mathbf{r})e^{-x_\sigma(\mathbf{r})}\right) \tag{5}$$

with b_σ being

$$b_\sigma(\mathbf{r}) = \left[\frac{x_\sigma^3(\mathbf{r})e^{-x_\sigma(\mathbf{r})}}{8\pi\rho_\sigma(\mathbf{r})}\right]^{1/3}. \tag{6}$$

x is solved by the nonlinear equation of

$$\frac{x_\sigma(\mathbf{r})e^{-(2/3)x_\sigma(\mathbf{r})}}{x_\sigma(\mathbf{r})-2} = \frac{2}{3}\pi^{2/3}\frac{\rho_\sigma^{5/3}(\mathbf{r})}{Q_\sigma(\mathbf{r})} \tag{7}$$

in which ρ_σ is the electron density, and

$$Q_\sigma = \frac{1}{6}(\nabla^2\rho_\sigma - 2\gamma D_\sigma), \tag{8}$$

$$D_\sigma = 2t_\sigma - \frac{1}{4}\frac{(\nabla\rho_\sigma)^2}{\rho_\sigma}, \tag{9}$$

$$t_\sigma = \frac{1}{2}\sum_{i\sigma}|\nabla\psi_{i\sigma}|^2. \tag{10}$$

The dependence of v_x^{BR} on the kinetic energy density t_σ makes it a meta-GGA potential. For finite systems $\gamma = 1$. For solids $\gamma = 0.8$ to fit the uniform electron gas limit.

Although it may be envisioned that all local or semilocal potentials including LDA/GGA/meta-GGA were short ranged, the Becke-Roussel'89 potential provides a counterexample. It is known that v_x^{BR} closely resembles Slater's averaged exchange potential [36]. For finite systems, the differences between the two potentials vanish at sufficiently large distance, which ensures that v_x^{BR} satisfies the correct asymptotic behavior of the exact exchange [2,27,37–39]:

$$v_x^{\mathrm{BR}}(r) \xrightarrow{r\to\infty} -\frac{1}{r}. \tag{11}$$

On the other hand, for solid surfaces the asymptotic behavior of v_x^{BR} is unknown and, like most other asymptotically long-ranged potentials, it has never been used for solid surfaces. In the following section, we show with accurate numerical results that for slab surfaces v_x^{BR} also satisfies the correct asymptotic behavior.

C. Computational details

Using the authentic slab geometry we have calculated six solid surfaces. In order to investigate the asymptotic behavior of the BR89 potential, the surfaces are intentionally chosen to be of different types including graphene (semimetal), ZnO $(10\bar{1}0)$ (large-gap insulator), ZnSe $(10\bar{1}0)$ (small-gap semiconductor), Si(111) (metal due to dangling bonds), Al (111) (metal due to nearly free electrons), and the jellium slab of $r_s = 3.0$ (model metallic surface), respectively. Details of the six surfaces can be found in Table I.

In all calculations the vacuum thickness is set to $D-d =$ 220 a.u. (or 116 Å). Note that to make a comparison to the supercell approach the top and bottom vacua need to be summed up. This gives the total vacuum thickness of 232 Å which would be very difficult to treat by the supercell approach.

All calculations proceed to self-consistency, with the final distance of both the electron density and the Kohn-Sham potential density being smaller than 0.01 a.u.. On the other hand, structural relaxation effects are ignored since they are irrelevant to the purpose of this work.

TABLE I. Details of the surfaces and values of the Becke-Johnson'89 exchange potential at the distance of 220 a.u. from the surface.

Surface	Slab thickness	v_x^{BR} (a.u.)
Graphene	One monolayer	−0.00465
ZnO$(10\bar{1}0)$	Four double layers	−0.00456
ZnSe$(10\bar{1}0)$	Four double layers	−0.00456
Si(111)	Five double layers	−0.00462
Al(111)	11 atomic layers	−0.00464
Jellium slab	10 a.u.	−0.00468

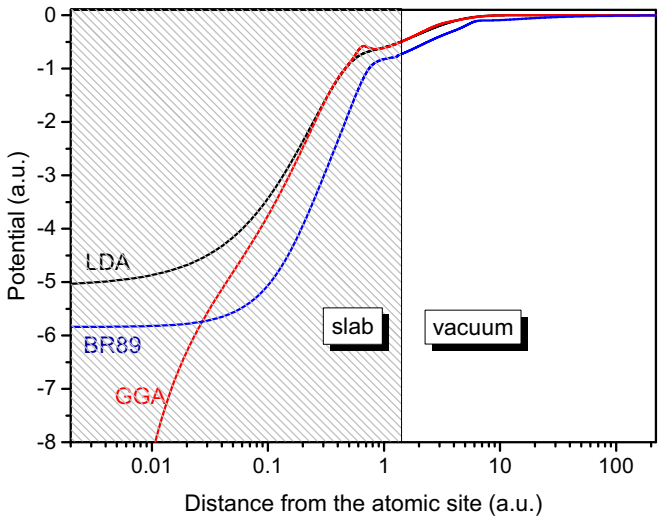

FIG. 2. (Color online) The Becke-Roussel'89 exchange potential and the LDA/GGA exchange-correlation potentials of graphene from one atomic site to the vacuum edge. The hatched region represents the slab (i.e., the interstitial region), and the rest is the vacuum. The edge of the slab is treated as the surface plane.

III. RESULTS AND DISCUSSIONS

A. The asymptotic behavior of the BR89 exchange potential

The Becke-Roussel'89 exchange potential of graphene is plotted in Figs. 2 and 3, starting from one atomic site up to the vacuum edge. The LDA/GGA potentials are also plotted for comparison.

Details of the potentials close to the nucleus can be seen from Fig. 2. At the nucleus the LDA potential is finite with a small slope [40], the GGA potential diverges, and the BR89 potential approaches a constant. There are two "bumps," or quick changes of slope, in the potential curves: One is within the 0.5–1.0 distance range and corresponds to the crossover from the $n = 1$ to the $n = 2$ shells. For this reason it is called a "shell structure." The other is within the 4.0–7.0 distance range which may relate to the "repulsive shoulder" in the EXX-OEP of jellium slabs [47]. However, it is known [13] that BR89 does not well reproduce the shell structures of the EXX-OEP. Therefore, in the rest of this paper we will bypass such details of BR89, and only focus on the vacuum part of this potential which is of interest in this work.

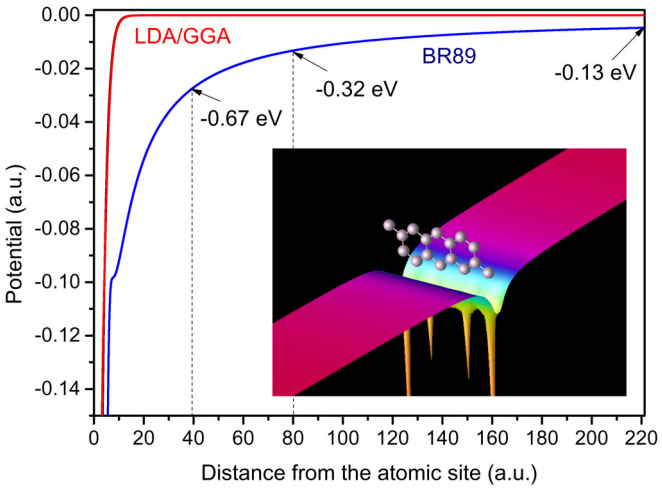

FIG. 3. (Color online) Same as Fig. 2 but distance in linear scale. The LDA/GGA potentials nearly coincide in the present scales. Values of v_x^{BR} at 20 and 40 Å from the atomic site and at the vacuum edge are highlighted. Inset: Rubber-sheet plot of v_x^{BR} in the slab and the near surface regions.

As can be seen from Fig. 3, away from the surface all potentials decay asymptotically to zero. The LDA/GGA decays are exponentially fast so that at the small distance of 10 Å from the surface both potentials already drop to practically zero. This explains why the supercell method works well with LDA/GGA since the total vacuum thickness can be safely set to only 20 Å.

On the other hand, at the same distance v_x^{BR} has barely entered the asymptotic region. The asymptotic decay of v_x^{BR} is very slow. Even at the doubled distance of 20 Å, the potential still has a large value of -0.63 eV. In an earlier attempt [3] to explore the image states of graphene, Silkin *et al.* used a huge supercell 85 Å thick. Their setup corresponds to the 42.5 Å distance in Fig. 3 at which $v_x^{\mathrm{BR}} = -0.32$ eV. In general, Figs. 2 and 3 clearly illustrate how hard it is for the supercell approach to handle asymptotically long-ranged potentials.

At the vacuum boundary v_x^{BR} reaches the value of -0.13 eV (or -0.00465 a.u.). This potential value is still significantly different form zero [41] despite that the density has dropped to 10^{-248}. Naturally, the extremely low electron density raises the concern whether this potential value is already ruined by numerical noises and therefore does not have real physical meaning. This is shown to be not so in Fig. 3 because v_x^{BR} varies smoothly all the way up to the vacuum edge. The absence of oscillatory noises in the potential curve indicates that the potentials computed by the authentic slab geometry are accurate and reliable.

Having finished analyzing graphene, let us now look at the BR89 potentials of all six surfaces plotted in Fig. 4. Note that Fig. 4 is made differently from Figs. 2 and 3 in two

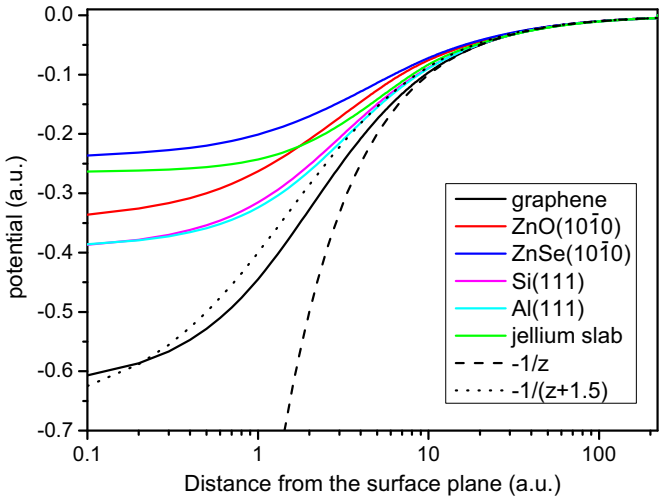

FIG. 4. (Color online) The Becke-Roussel'89 exchange potentials of the six slabs from the surface plane to the vacuum edge. Dashed lines show the analytical relations of $v(z) = -1/z$ and $v(z) = -1/(z + 1.5)$.

aspects: First, the potentials in Fig. 4 are now x,y averaged. For graphene this means the "bumps" mentioned earlier are smeared out. Second, to facilitate comparison to the asymptotic behavior, $z = 0$ is now set to the surface plane rather than to one atomic site. Since the exact location of the surface plane is not well defined, for all six slabs it is chosen to be the interstitial edge (see Fig. 1).

Figure 4 shows that in the near surface region the six potentials differ appreciably. On the other hand, starting from a distance of 40 a.u. away all potentials converge to the $-1/z$ asymptotic behavior. In Fig. 4, the distance at which the asymptotic behavior is reached is system dependent, which vaguely defines "the boundary of the asymptotic region." For graphene, the location of the boundary in Fig. 4 seems to be much further than what is found by Engel [28], who claimed that EXX-OEP already reaches $-1/z$ before 10 a.u. Although part of the difference is due to the fact that BR89 is only an approximated exchange potential which is not expected to match the EXX-OEP in the near surface region, the main reason for the difference is due to different $z = 0$ settings in the two works: In Fig. 4 $z = 0$ is set to the surface plane, while in Engel's work it is set to the center of the slab. Correspondingly, the absolute value of z in Fig. 4 equals to $z + d$ (d is half the interstitial thickness; see Fig. 1) in Engel's work.

In Fig. 4, the BR89 potential of graphene is compared to both $-1/z$ and $-1/(z + d)$, with $d = 1.5$ being the value for graphene. Naturally, BR89 fits to the latter function better in close distance because $-1/(z + d)$ does not diverge at $z = 0$ (as $-1/z$ does). As to the boundary of the asymptotic region, there is no strict definition of its exact location. Nevertheless, the term "asymptotic region" itself implies that its boundary shall be insensitive to the two different settings of $z = 0$. In Fig. 4, $-1/z$ and $-1/(z + d)$ start to merge also at about 40 a.u., while at 8.5 a.u. (corresponding to 10 a.u. in Engel's work) they still differ appreciably, implying that the boundary of the asymptotic region is not as close as it is claimed before.

The values of v_x^{BR} at the vacuum edge of the six surfaces are listed in Table I. Surprisingly, in all cases $v_x^{\mathrm{BR}} \approx -0.0046$ despite that the surfaces belong to very different types. The question is then why.

The answer can be found by recalling the asymptotic behaviors of the exact DFT exchange-correlation potential, a topic having been disputed for many years and is still far from being settled [37,42,43,47]. In particular, there has been lack of rigorous mathematical proofs to the asymptotic behaviors of semi-infinite surfaces suggested by Lang and Kohn [1] and by Almbladh and von Barth [2]. On the other hand, for slab surfaces the issue for exchange is resolved. Horowitz *et al.* [33] pointed out that for jellium slabs the exchange potential decays as

$$v_x(z) \xrightarrow{z\to\infty} -\frac{1}{z}. \tag{12}$$

This relation was later derived analytically by Engel [28,44], who found that it is actually universal for slabs of arbitrary types irregardless of their chemical composition or physical properties (e.g., whether they are metals or semiconductors). Setting $z = 220$ in Eq. (12) gives $v_x = -0.00455$, which immediately explains our results in Table I. The remaining, small differences are because Eq. (12) is strict only when the vacuum edge is infinitely far away from the surfaces.

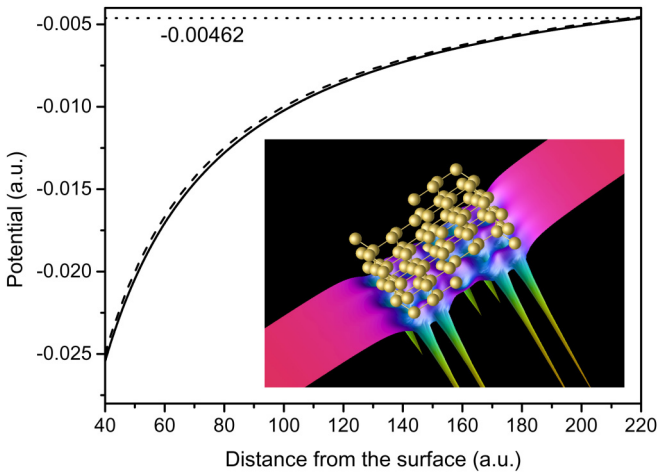

FIG. 5. (Color online) The Becke-Roussel'89 exchange potential of the Si(111) surface in the asymptotic region (solid line) compared to the asymptotic behavior of the exact exchange, $v(z) = -1/z$ (dashed line). Inset: Rubber-sheet plot of v_x^{BR} in the slab and the near surface regions.

To get a closer look at the asymptotic behavior of the BR89 potential, in Fig. 5 we compare the BR89 potential of the Si(111) surface to the analytic relation of Eq. (12) in the asymptotic region. Although in the near surface region BR89 differs appreciably from Eq. (12) (see Fig. 4), starting from $z = 40$ up to the vacuum edge the two curves match each other very well at the present scales. Therefore, all our results clearly show that the BR89 potential satisfies the correct asymptotic behavior, Eq. (12), for slab surfaces.

B. Implications to the supercell approach

The above results help to understand the use of long-ranged potentials within the supercell approach. Let $\psi_{n\mathbf{k}}^{(i)}(z), \rho^{(i)}(z), v^{(i)}(z)$ be the Kohn-Sham orbital, the density, and the potential of the ith supercell solved by the authentic slab geometry (to facilitate discussion the x,y coordinates have been suppressed), and assume the size of the supercell has been chosen large enough to enclose all orbitals in concern. Then the density and the Coulomb potential are essentially restricted within the same supercell. The exchange-correlation potential, on the other hand, can still penetrate from neighboring supercells so that the interslab interactions can be roughly expressed as

$$\left\langle \psi_{n\mathbf{k}}^{(i)}(z) \middle| v_{xc}^{(i+1)}(z) \middle| \psi_{n\mathbf{k}}^{(i)}(z) \right\rangle. \tag{13}$$

The reason why the BR89 potential is long ranged is because it is the Coulomb potential of the exchange hole: Even if the hole density is restricted within one supercell, its Coulomb potential still extends to infinity.

To avoid the interslab interactions, one either uses huge supercell or truncates the v_{xc} as

$$v_x^{(i)}(z) \longrightarrow \begin{cases} v_x^{(i)}(z) & \text{(within the supercell)} \\ 0 & \text{(out of the supercell).} \end{cases} \tag{14}$$

This truncation scheme is similar to existing ones [45,46,48,49], and with it the minimum size of

the supercell is then determined by the extension of all orbitals in concern: For ground state properties, only the occupied orbitals matter; for excited state properties such as response functions, the unoccupied orbitals are more delocalized and therefore the size of the supercell must be increased accordingly. As to image states, since they are bound by the long-ranged tail of the potential, they are very sensitive to truncation at any finite distance. To describe image states correctly an extremely large supercell is needed.

IV. SUMMARY

In this work, we have addressed the problem of surface calculations using asymptotically long-ranged potentials. While the supercell approach is intrinsically inferior for such jobs, we have shown that the authentic slab geometry of FLAPW, which is based on the linearization technique for vacuum, provides an excellent solution. Within this approach, calculations with asymptotically long-ranged potentials are as easy as with short-ranged LDA/GGA, and the size of the basis set, the computational cost, and the convergence speed are all essentially the same. Therefore, the authentic slab geometry is a very useful tool for surface calculations with both short- and long-ranged potentials, including especially the asymptotically correct exchange-correlation potentials [5–15], the long-range corrected potentials of hybrid functionals [16–23], *GW* approximation [29], etc.

We have used the Becke-Roussel'89 potential to calculate six solid surfaces of different types. We have shown that accurate potential values can be obtained by the authentic slab geometry more than 100 Å away from the surfaces, even though the electron density has become extremely low. Previously, the Becke-Roussel'89 potential is known to satisfy the correct asymptotic behavior for finite systems. This work further established that it also satisfies the correct asymptotic behavior for slab surfaces. For jellium slabs, Horowitz *et al.* [33] have identified that the asymptotic behavior comes from the Slater component of the EXX-OEP. Our results imply that the same conclusion in fact holds for arbitrary slabs. On the other hand, for surfaces of semi-infinite jellium the Slater component of EXX-OEP ceases to be responsible for the asymptotic behavior of exchange. Correspondingly, for surfaces of semi-infinite materials the asymptotic behavior of BR89 is not likely correct.

One possible application of the Becke-Roussel'89 potential is to combine it with any short-ranged potentials (for example, LDA/GGA, or range separated hybrid functionals, etc.) to build asymptotically correct model exchange potentials, which can be used for both finite systems and slab surfaces.

ACKNOWLEDGMENTS

This work is supported by the Ministry of Science and Technology of China (Grants No. 2011CB933001 and No. 2011CB933002), and by the National Natural Science Foundation of China (Grants No. 91221202 and No. 91421303).

[1] N. D. Lang and W. Kohn, Phys. Rev. B **1**, 4555 (1970).
[2] C.-O. Almbladh and U. von Barth, Phys. Rev. B **31**, 3231 (1985).
[3] See, for an example, V. M. Silkin, J. Zhao, F. Guinea, E. V. Chulkov, P. M. Echenique, and H. Petek, Phys. Rev. B **80**, 121408(R) (2009).
[4] M. Levy, J. P. Perdew, and V. Sahni, Phys. Rev. A **30**, 2745 (1984).
[5] R. van Leeuwen and E. J. Baerends, Phys. Rev. A **49**, 2421 (1994).
[6] C. R. Pan, P.-T. Fang, and J.-D. Chai, Phys. Rev. A **87**, 052510 (2013).
[7] D. J. Tozer and N. C. Handy, J. Chem. Phys. **109**, 10180 (1998).
[8] D. J. Tozer, J. Chem. Phys. **112**, 3507 (2000).
[9] P. R. T. Schipper, O. V. Gritsenko, S. J. A. van Gisbergen, and E. J. Baerends, J. Chem. Phys. **112**, 1344 (2000).
[10] M. E. Casida and D. R. Salahub, J. Chem. Phys. **113**, 8918 (2000).
[11] M. Grüning, O. V. Gritsenko, S. J. A. van Grisbergen, and E. J. Baerends, J. Chem. Phys. **114**, 652 (2001).
[12] Q. Wu, P. W. Ayers, and W. T. Yang, J. Chem. Phys. **119**, 2978 (2003).
[13] A. D. Becke and E. R. Johnson, J. Chem. Phys. **124**, 221101 (2006).
[14] X. Andrade and A. Aspuru-Guzik, Phys. Rev. Lett. **107**, 183002 (2011).
[15] A. P. Gaiduk, D. S. Firaha, and V. N. Staroverov, Phys. Rev. Lett. **108**, 253005 (2012).
[16] A. Savin, in *Recent Developments and Applications of Modern Density Functional Theory*, edited by J. M. Seminario (Elsevier, Amsterdam, 1996), p. 327.
[17] H. Iikura, T. Tsuneda, T. Yanai, and K. Hirao, J. Chem. Phys. **115**, 3540 (2001).
[18] T. Yanai, D. P. Tew, and N. C. Handy, Chem. Phys. Lett. **393**, 51 (2004).
[19] O. A. Vydrov, J. Heyd, A. V. Krukau, and G. E. Scuseria, J. Chem. Phys. **125**, 074106 (2006).
[20] E. Livshits and R. Baer, Phys. Chem. Chem. Phys. **9**, 2932 (2007).
[21] J.-D. Chia and M. Head-Gordon, J. Chem. Phys. **128**, 084106 (2008); Phys. Chem. Chem. Phys. **10**, 6615 (2008); Chem. Phys. Lett. **467**, 176 (2008); J. Chem. Phys. **131**, 174105 (2009).
[22] Y.-S. Lin, C.-W. Tsai, G.-D. Li, and J.-D. Chai, J. Chem. Phys. **136**, 154109 (2012).
[23] Y.-S. Lin, G.-D. Li, S.-P. Mao, and J.-D. Chai, J. Chem. Theory, Comput. **9**, 263 (2013).
[24] T. Kotani, Phys. Rev. Lett. **74**, 2989 (1995).
[25] M. Städele, J. A. Majewski, P. Vogl, and A. Görling, Phys. Rev. Lett. **79**, 2089 (1997).
[26] R. T. Sharp and G. K. Horton, Phys. Rev. **90**, 317 (1953).
[27] J. D. Talman and W. F. Shadwick, Phys. Rev. A **14**, 36 (1976).
[28] E. Engel, J. Chem. Phys. **140**, 18A505 (2014).
[29] L. Hedin, Phys. Rev. **139**, A796 (1965).
[30] H. Krakauer, M. Posternak, and A. J. Freeman, Bull. Am. Phys. Soc. **23**, 258 (1978); M. Posternak, H. Krakauer, A. J. Freeman,

and D. D. Koelling, *ibid.* **23**, 259 (1978); H. Krakauer, M. Posternak, and A. J. Freeman, Phys. Rev. B **19**, 1706 (1979).
[31] O. Jepsen, J. Madsen, and O. K. Andersen, Phys. Rev. B **18**, 605 (1978).
[32] A. D. Becke and M. R. Roussel, Phys. Rev. A **39**, 3761 (1989).
[33] C. M. Horowitz, C. R. Proetto, and J. M. Pitarke, Phys. Rev. B **81**, 121106(R) (2010).
[34] E. Wimmer, H. Krakauer, M. Weinert, and A. J. Freeman, Phys. Rev. B **24**, 864 (1981).
[35] L.-H. Ye, Phys. Rev. B **91**, 075101 (2015).
[36] J. C. Slater, Phys. Rev. **81**, 385 (1951).
[37] L. J. Sham, Phys. Rev. B **32**, 3876 (1985).
[38] M. K. Harbola and V. Sahni, Phys. Rev. Lett. **62**, 489 (1989).
[39] E. Engel, J. A. Chevary, L. D. Macdonald, and S. H. Vosko, Z. Phys. D **23**, 7 (1992).
[40] Z. Qian and V. Sahni, Phys. Rev. A **75**, 032517 (2007).
[41] In general there is no limitation on the vacuum thickness in the authentic slab geometry. In the present work, the vacuum thickness cannot exceed 220 a.u. But the limit comes from the BR89 potential rather from the authentic slab geometry itself. Setting the vacuum thickness too large would cause underflow of some quantities in Eqs. (5)–(10). Although with higher precision the vacuum thickness can be further increased, we choose not to do so since all our conclusions are already clear enough with our present results.
[42] A. G. Eguiluz, M. Heinrichsmeier, A. Fleszar, and W. Hanke, Phys. Rev. Lett. **68**, 1359 (1992).
[43] M. K. Harbola and V. Sahni, Phys. Rev. B **39**, 10437 (1989).
[44] E. Engel, Phys. Rev. B **89**, 245105 (2014).
[45] C. A. Rozzi, D. Varsano, A. Marini, E. K. U. Gross, and A. Rubio, Phys. Rev. B **73**, 205119 (2006).
[46] S. Ismail-Beigi, Phys. Rev. B **73**, 233103 (2006).
[47] C. M. Horowitz, C. R. Proetto, and S. Rigamonti, Phys. Rev. Lett. **97**, 026802 (2006).
[48] V. U. Nazarov, New J. Phys. **17**, 073018 (2015).
[49] V. U. Nazarov, F. Alharbi, T. S. Fisher, and S. Kais, Phys. Rev. B **89**, 195423 (2014).